SUPPLEMENTARY INFORMATION

(S-1) Materials and Methods

Animal care: Sixty adult male Sprague Dawley rats [weighing 316 ± 27g (mean ± SD)] were cared for at University of Kentucky Division of Laboratory Animal Resources facility under a 12:12 h light: dark cycle at 21 ^{o}C and 30 to 70% humidity. All rats had *ad libitum* access to 2018 Harlan diet and reverse osmosis water. Animal work was approved by the University of Kentucky Institutional Animal Care and Use Committee. The research was conducted in accordance with the Guiding Principles in the Use of Animals in Toxicology.

Ceria Infusion: A cannula was surgically inserted, under sterile conditions, into each of the femoral veins and extended into the vena cava. The following day, un-anesthetized rats were iv-infused via the shorter cannula with a ceria dispersion (85 mg ceria/kg), or water (controls) adjusted to pH 3.9 with citric acid, concurrently with an equal volume and rate of 1.8% saline infused into the second cannula to achieve net infusion of iso-isomotic solution. Each fluid was iv-infused at rates of 2 ml/kg/h over a duration of 1 h. Ceria iv-infused rats were terminated at 1 h [n=5], 20 h [n=5], 30 days [n=14], or 90 days [n=7] and the number of control rats was 5, 8, 10, and 6 respectively. The cannulae were surgically removed from 30 and 90 day rats. Physiological statuses including respiratory, neurological, ophthalmic, gastrointestinal of both control and treated rats held for 30 and 90 days were assessed daily (cage-side observations).

Animal termination, tissue processing, and histopathology analysis: After termination of ketamine/xylazine-anesthetized rats, tissues of liver, lung, kidney, spleen, heart, thymus, and brain were processed for histopathology analysis.

(S-2) Microscopy:

Thin tissue sections (~ 3 mm^2) were immersion fixed (24h; dehydrated in ascending concentrations of ethanol; embedded in Araldite 502.). Sections were stained with hematoxylin (H) and eosin (E) and screened for CeO_2-NPs-containing Kupffer cells (Fig. S-II b) using a Nikon Eclipse E-800 microscope and software to tabulate size and density of lesions inside liver. Nanoceria-induced cellular degeneration and proliferation in liver tissue were determined by TUNEL and proliferating cell nuclear antigen (PCNA) immunostaining. The general cytoarchitecture of the liver was not altered by the sequestered CeO_2-NPs, but hepatocellular cords were parted by sinusoids and Kupffer cells contained many CeO_2-NPs which added granularity that was seen with light microscopy after H & E staining. After the 90 days Kupffer cells with mononucleated lymphocytes had formed large granulomata in the tissue parenchyma (Fig. S-II a). Electron dense nanoceria was easily seen inside Kupffer cells, typically forming small CeO_2-agglomerates (Fig. S-II b), but surrounding hepatocytes rarely showed cytoplasmic inclusion of CeO_2-agglomerates. Any CeO_2-agglomerates were typically surrounded by stacks of rough endoplasmic reticulum (Fig. S-II c). In both the Kupffer cells and the hepatocytes, the internalized ceria agglomerated and underwent fusion with lysosomes to form phagolysosome. Besides the ceria nanocubes of varying sizes, a range of spherical to oblong shaped proteinaceous inclusions also appeared in the matrix of the phagolysosomes (Fig. S-II d). In CeO_2- retained hepatocytes, the CeO_2-NP-containing lysosomal complex typically pointed towareds the surface of the bile canaliculi (no CeO_2-NPs were observed in bile canaliculi or bile ducts).

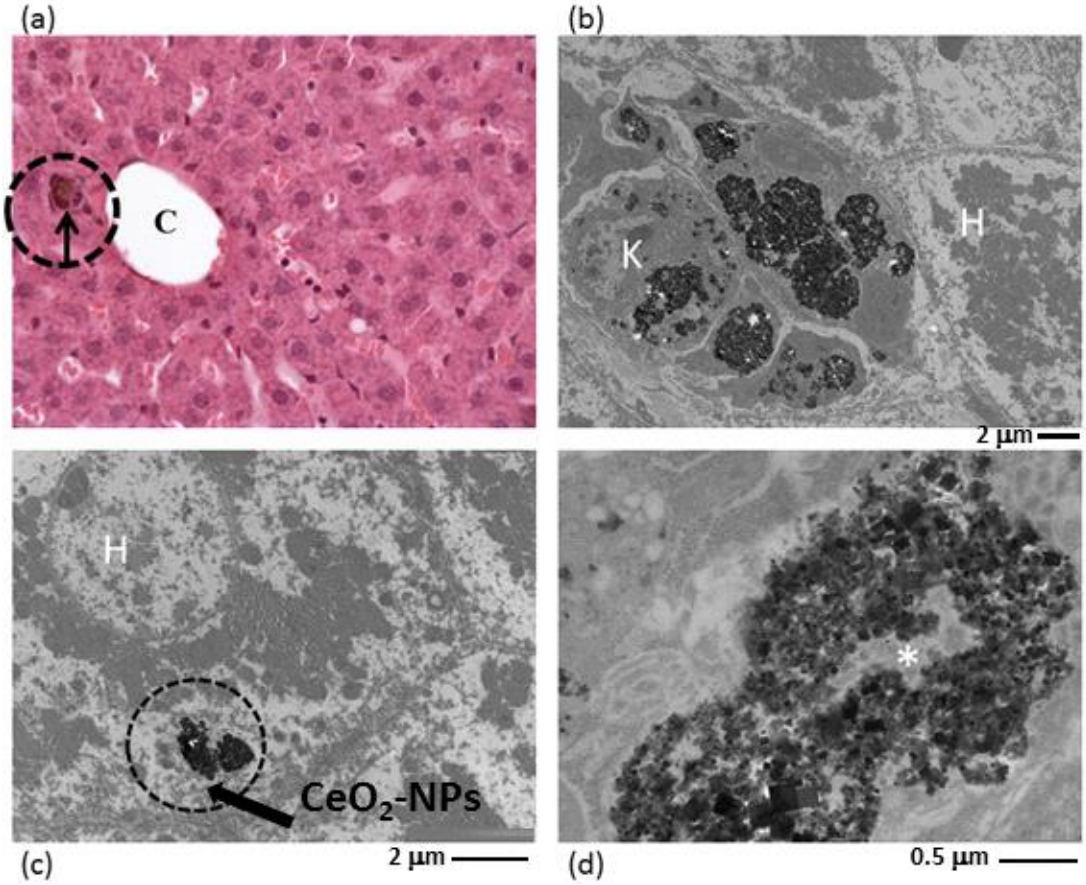

Figure S-II a-d

(a) In the well preserved liver parenchyma a granuloma (arrow) formed adjacent to a central vein (C), H&E stain.

(b) In a hepatic sinusoid several ceria containing Kupffer cells [K] formed a granuloma. Note the adjacent hepatocytes [H] are ceria free.

(c) Smaller agglomerates of ceria [arrow] are more frequently observed in hepatocytes.

(d) Large phagolysosome containing ceria nanoparticles of varying sizes is shown. Note small proteinaceous materials [*] formed between nanoceria clusters.

(S-3) **HRTEM**

Selected blocks were prepared into thin sections (800 Å) and collected on Formvar/carbon coated copper grids (200-mesh, Ted Pella Inc. Redding, CA) without staining. TEM imaging was performed using a FEI Tecnai F20 field-emission gun transmission electron microscope (accelerating voltage of 200 kV). A symmetrical multi-beam illumination was used for high-resolution TEM (HRTEM). Images were recorded using a Gatan Ultrascan 4k x 4k CCD camera and data processing and analysis was done using Gatan Digital Micrograph software.

Differences between liver and spleen: In-vivo processing of CeO_2-NPs inside liver (Fig. S-III a,b) was compared with those inside spleen (Fig. S-III c) and demonstrate much greater amounts of CeO_2-clouds are present in the rat liver after 90 days.

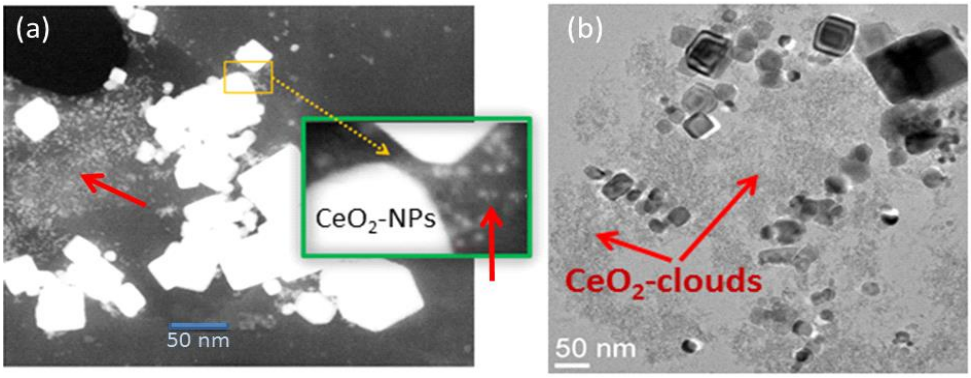

Fig. S- III a, b *CeO_2-clouds in liver: a) STEM image and b) HRTEM*

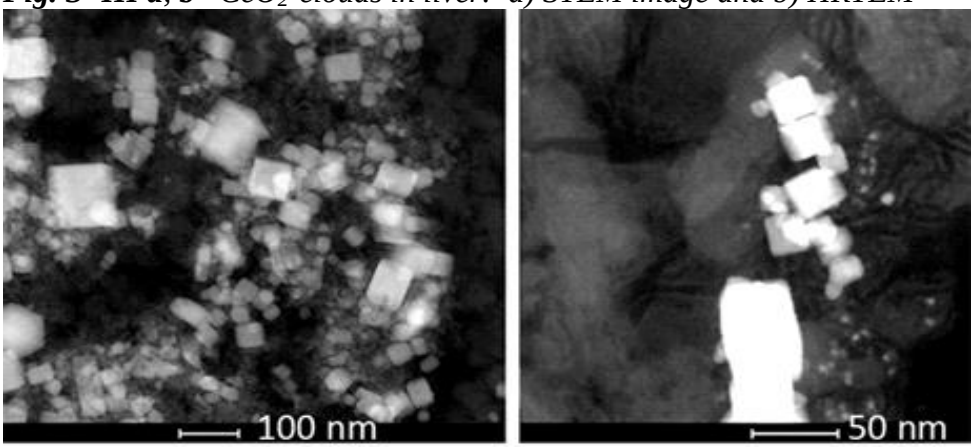

Fig. S- III c *CeO_2-NPs in spleen (STEM imaging).*

(S 4) Ce- and P –Needles and Rods in Rat Liver

Ce-phosphate needles and rods may have formed from Ce- and phosphate ions available inside the liver and the crystallites are shown in Fig. S-V; both Ce and P are evident in the accompanying EDX spot analysis.

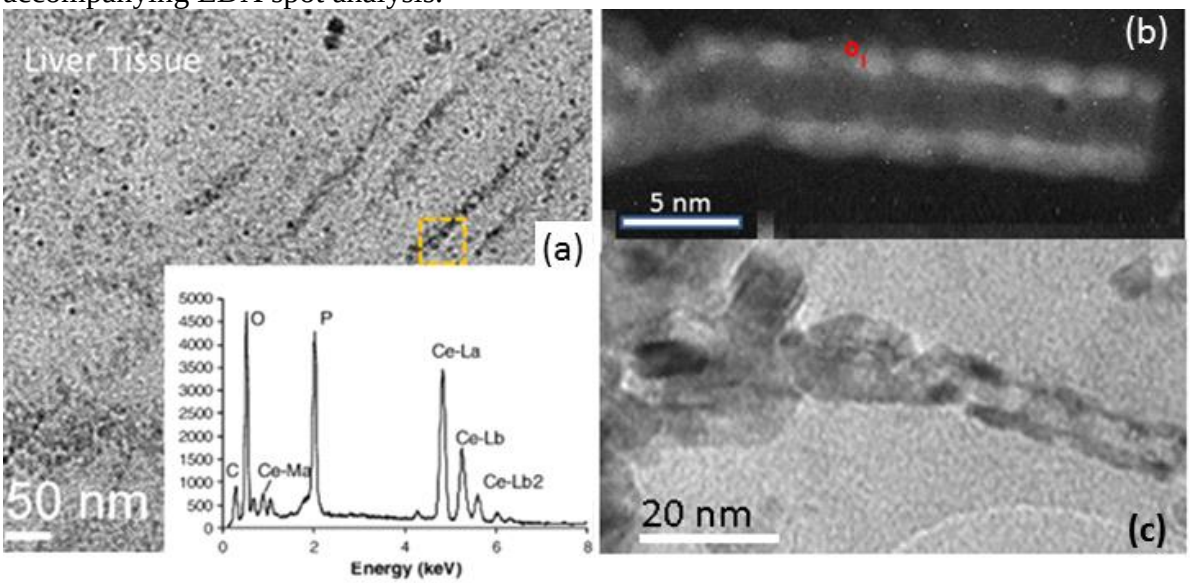

Fig. S-IV a,b,c *a) needle-shaped Ce-phosphate; b) rod-shaped Ce-phosphate with individual CeO_2 crystallites; c) Ce-phosphate rods with CeO_2-NPs.*

(S-5) STEM and EELS

To study the oxidation/reduction of ceria at the nanoscale, Electron Eenergy Loss Spectroscopy (EELS) analyses were performed in STEM (scanning) mode using 1 nm probe size. To position the probe and collect the EELS spectrum from specific crystallites, a STEM image was first acquired at a Fischione High-Angle Annular Dark Filed Detector (EELS-spectra were collected using a 1024-channel Gatan Image Filter). The spectral resolution estimated from the full width at half maximum of the zero-loss peak was about 0.8 eV. An energy dispersion of 0.2 eV/ channel, and an energy offset of 800 eV were selected to acquire the cerium M4,5-edge. EELS-spectra containing absorption edges specific to ceria were recorded using an alpha of 30 mrad, and a beta of 6 mrad. To minimize any possible electron beam interaction that could reduce cerium (IV) ions to the Ce (III), a less-focused beam was used. The EDX spectrum taken over a larger area of the grains also had a peak associated with P and there may have been Ce-phosphates present inside the larger grains.

(S-6) X-ray Photoelectron Spectroscopy

VG Scientific MultiLab 3000 ultra-high vacuum surface analysis system, operating at the base pressure in the 10^{-8} Torr range and equipped with dual-anode (Mg/Al) X-ray source and CLAM4 hemispherical electron energy analyzer, was used for this study. Non-monochromatized Mg Kα X-ray beam ($h\nu \approx 1253.6$ eV) was used as the source and XPS spectra were collected at an electron emission angle of 54.7^{o} relative to the surface normal. High resolution spectra were collected on synthesized ultra-fine CeO_2-NPs (Fig. S-VIa) and with PAS energy of 50 eV (Fig. S-7). Six peaks associated with Ce^{4+} and four with Ce^{3+} were used for the deconvolution and a series of spectra were acquired at different stages of the redox cycle (Fig. S-VI b). The Ce^{3+}/Ce^{4+} ratios and concentration of Ce^{3+} were determined using integrated peak areas in (eq. S-VI).

(eq. S-VI) $[Ce^{3+}] = I(Ce^{3+})/(I(Ce^{3+})+ I(Ce^{4+}))$

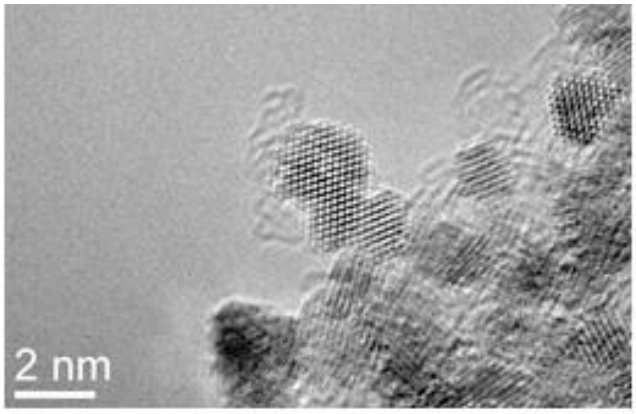

Fig S-VI a *Synthesized ultra-fine CeO_2-NPs*

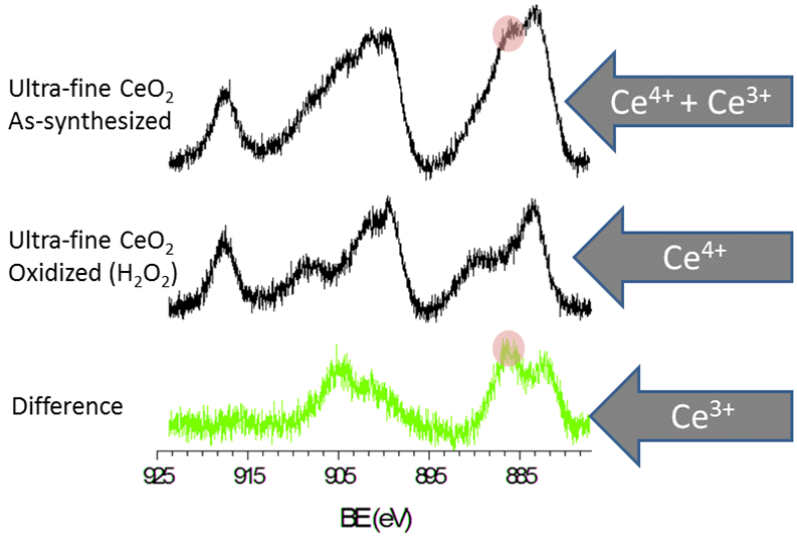

Fig. S-VI b *XPS survey-spectrum of ultra-fine ceria after synthesis (top), after oxidation with H_2O_2 (middle) and difference in Ce^{3+} (bottom). The red dots show Cd^{3+} peaks missing in oxidized ceria (middle).*